ACS APPLIED MATERIALS & INTERFACES

Research Article

Cite This: ACS Appl. Mater. Interfaces XXXX, XXX, XXX−XXX

www.acsami.org

Ultrafast Three-Dimensional Printing of Optically Smooth Microlens Arrays by Oscillation-Assisted Digital Light Processing

Chao Yuan,[†] Kavin Kowsari,[†] Sahil Panjwani,[†] Zaichun Chen,[†] Dong Wang,[†] Biao Zhang,[†] Colin Ju-Xiang Ng,[†] Pablo Valdivia y Alvarado,[†] and Qi Ge*[,†,‡]

[†]Digital Manufacturing and Design Centre, Singapore University of Technology and Design, Singapore 487372, Singapore

[‡]Department of Mechanical and Energy Engineering, Southern University of Science and Technology, Shenzhen 518055, China

Supporting Information

ABSTRACT: A microlens array has become an important micro-optics device in various applications. Compared with traditional manufacturing approaches, digital light processing (DLP)-based printing enables fabrication of complex three-dimensional (3D) geometries and is a possible manufacturing approach for microlens arrays. However, the nature of 3D printing objects by stacking successive 2D patterns formed by discrete pixels leads to coarse surface roughness and makes DLP-based printing unsuccessful in fabricating optical components. Here, we report an oscillation-assisted DLP-based printing approach for fabrication of microlens arrays. An optically smooth surface (about 1 nm surface roughness) is achieved by mechanical oscillation that eliminates the jagged surface formed by discrete pixels, and a 1−3 s single grayscale ultraviolet (UV) exposure that removes the staircase effect. Moreover, computationally designed grayscale UV patterns allow us to fabricate microlenses with various profiles. The proposed approach paves a way to 3D print optical components with high quality, fast speed, and vast flexibility.

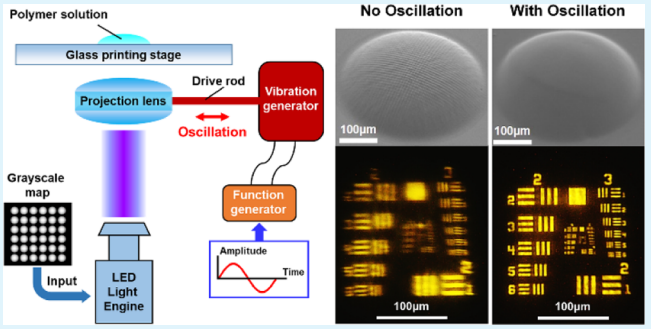

KEYWORDS: *microlens array, digital light processing, oscillation, optical surface roughness, grayscale*

INTRODUCTION

With increasing demand on the miniaturization of optoelectronics, microlens array[1,2] has attracted significant attention and become an important micro-optics device widely used in compact imaging,[3,4] sensing,[5,6] optical communication,[7] charge-coupled devices (CCDs),[8] three-dimensional (3D) displays,[9] and others.[10,11] Typically, microlens array consists of multiple micron sized lenses with optical surface smoothness and superior uniformity, which raises high requirement on machining precision. In the past decades, a variety of manufacturing techniques have been developed including thermal reflow of photoresist,[12−14] microdroplet jetting,[15] direct laser writing,[16−19] hot embossing,[20] and others.[21−23] Despite tremendous progress, there still exist some limitations for these techniques such as high time consumption,[16,17] high process complexity,[20] lack of fabrication flexibility,[12,13] and difficulty in consistency control.[15]

Digital light processing (DLP)-based 3D printing is a high-resolution, high-throughput, and low-cost manufacturing technology that creates free-form solid 3D geometries through the localized photo-polymerization process triggered by projection of digitally modulated ultraviolet (UV) patterns onto liquid polymer solution. In a DLP-based 3D printer, the digital micromirror device (DMD) that precisely switches on and off about a million micromirrors with high frequency digitalizes light illumination in location and intensity, and therefore enables grayscale modulation at pixel size level.[24] In recent years, the remarkable advances make DLP-based 3D printing capable of creating geometrically complex 3D structures,[25−29] and an ideal manufacturing approach for a wide range of applications from micro to mesoscales.[24−26] However, the way that the DLP-based 3D printing creates 3D geometries by stacking successive 2D patterns formed by discrete pixels leads to microscale (about the pixel size and layer thickness) surface roughness. This relatively coarse surface roughness fails to satisfy the sub 10 nm surface roughness requirement of optical elements, and results in few successful examples of manufacturing optic components,[30−32] particularly microlenses, through DLP-based 3D printing.

Here, we present an oscillation-assisted DLP-based 3D printing approach that enables fabrication of microlens arrays with optically smooth surface via a single 1−3 s exposure of grayscale UV light. Computationally designed grayscale patterns are employed to realize microlens profiles upon one single UV exposure which removes the staircase effect existing in the traditional layer-by-layer 3D printing manner. To further

Received: August 16, 2019
Accepted: October 7, 2019
Published: October 7, 2019

DOI: 10.1021/acsami.9b14692
ACS Appl. Mater. Interfaces XXXX, XXX, XXX−XXX

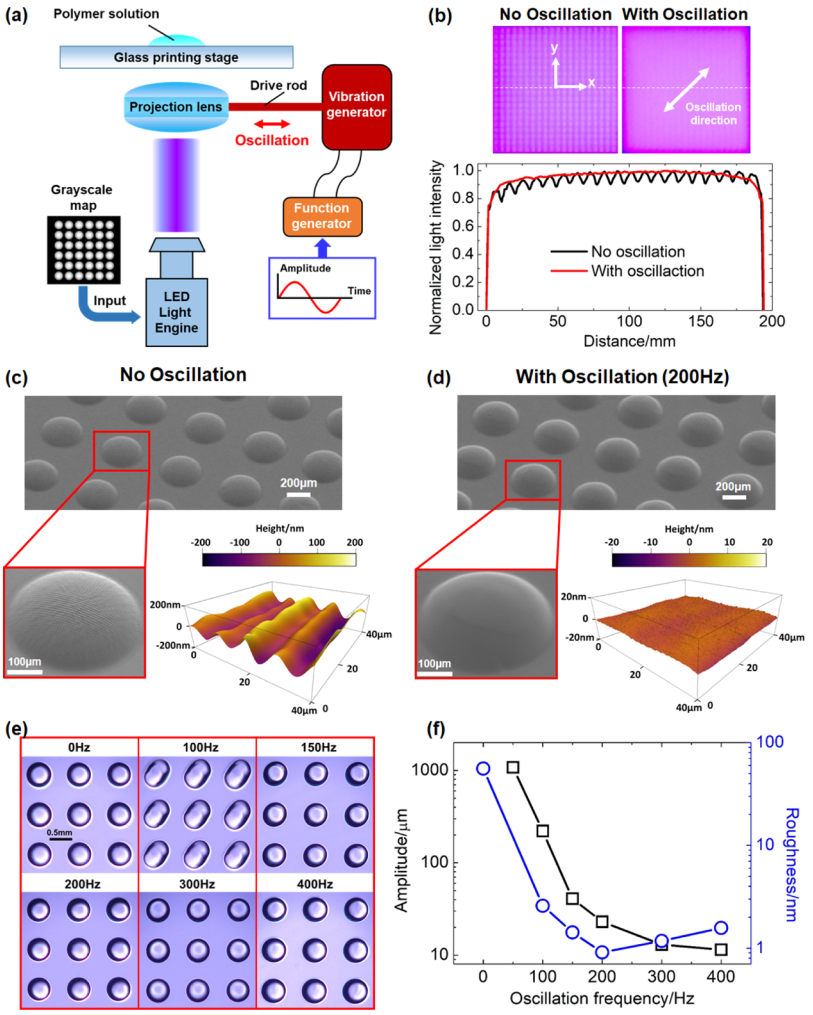

Figure 1. Fabrication of microlens array by an oscillation-assisted DLP-based printing system. (a) Schematic of the oscillation-assisted DLP-based printing system. (b) Comparison of the projection pattern (200 μm × 200 μm) and normalized light intensity distribution between nonoscillated and oscillated projection. (c,d) Scanning electron microscopy (SEM) and atomic force microscopy (AFM) characterizations of the microlens arrays fabricated under nonoscillated and oscillated projection. (e) Top view images of microlens arrays fabricated under elevated oscillation frequencies. (f) Relationship between oscillation amplitude and oscillation frequency of the current setup, and the corresponding effect on the surface roughness of the fabricated microlenses.

eliminate the jagged surface formed because of the gaps between the discrete pixels, mechanical oscillation is applied to the projection lens. About 1 nm surface roughness of printed microlenses is ensured by the combination of mechanical oscillation and single grayscale UV exposure. Furthermore, DMD enables UV radiation with different patterns and grayscale, therefore allows us to fabricate microlenses with various profiles and curvatures upon one single exposure. Overall, oscillation-assisted DLP-based 3D printing along with computationally designed UV patterns renders an ultrafast and flexible approach to fabricate microlens arrays with an optically smooth surface, and paves a way to 3D print optical components with high quality, fast speed, and vast flexibility.

RESULTS AND DISCUSSION

Figure 1a presents the schematic of an oscillation-assisted DLP-based printing system that mainly consists of a digital light engine, a projection lens, glass printing stage, and oscillation system. During printing, 405 nm near UV patterns comprised of about a million 10 μm × 10 μm pixels controlled by equal amounts of micromirrors in DMD are projected upward through a projection lens and focused on the top surface of the glass printing stage where a droplet of photocurable polymer solution is placed. The drive rod of a single-directional linear vibration generator is firmly attached to the projection lens to oscillate projected UV patterns in sinusoidal mode where amplitude and frequency are controlled by a function generator. The oscillation is performed along the diagonal direction of projection area (Figure 1b). In principle, the oscillator can also be attached to the glass printing stage or LED light engine to achieve the same effect. However, in reality, the vibration of the glass printing stage will result in the unwanted motion of the polymer solution sitting on it; and because the LED light engine is a complex and precise optical instrument, the vibration on it may cause unexpected failure of the system and unnecessary economic loss.

To examine the effect of mechanical oscillation on quality of projected patterns, we used a complementary metal oxide semiconductor sensor of a digital camera (D810, Nikon Corp., Tokyo, Japan) to measure the planar light intensity variation within a 200 μm × 200 μm square pattern. When the oscillation is off, the projected pattern exhibits a checkerboard

DOI: 10.1021/acsami.9b14692
ACS Appl. Mater. Interfaces XXXX, XXX, XXX−XXX

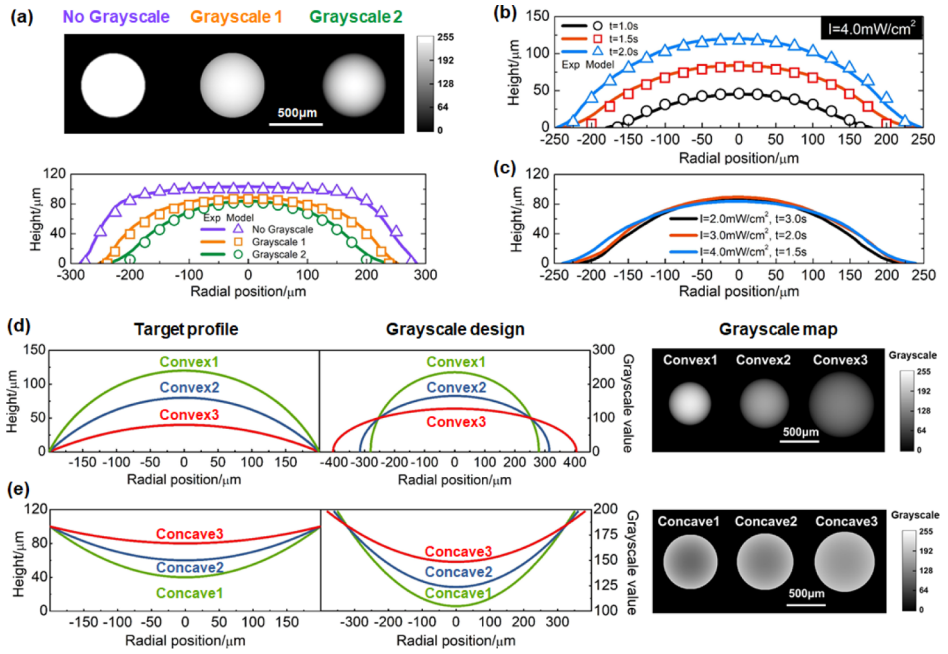

Figure 2. Morphological characterization and computational design of microlens profiles. (a) Profiles of the microlenses fabricated under different grayscale projection. (b) Profiles of the microlenses fabricated under a given light intensity with different exposure durations. (c) Profiles of the microlenses fabricated under a given light dose. (d) Grayscale design for convex microlens profiles with the same diameter and different curvatures. (e) Grayscale design for concave microlens profiles with the same diameter and different curvatures.

pattern where the square is discretized by 20 × 20 pixels, and the dark grids between pixels can be clearly observed (Figure 1b). These dark grids are caused by the small gaps between neighboring micromirrors that reduce the local light intensity, thereby resulting in the nonuniform light intensity distribution measured in Figure 1b. In contrast, the projection lens oscillation smears the discrete pixels and eliminates the dark grids between pixels. We further compare the light intensity variation along the middle line of projected patterns. When the oscillation is off, the light intensity fluctuation due to the discrete pixels can be clearly seen, whereas the projection lens oscillation eliminates the light intensity fluctuation and unifies the light intensity within the square (Figure 1b). In addition, as shown in Figure 1b, we set the oscillation along the diagonal direction so that the projection lens oscillation could equally smear the discrete pixels in both x and y directions.

To investigate the surface roughness improvement by the application of projection lens oscillation, we printed microlens arrays by projecting arrays of grayscale circles with/without oscillation. The SEM images in Figure 1c,d reveal that the grayscale projection enables us to create convex microlenses wherever the oscillation is applied or not. However, upon comparing the surface roughness of a single microlens, we find that the projection lens oscillation removes the jagged surface. Furthermore, we quantify the surface roughness via atomic force microscopy (AFM). For each measurement, we scanned an area of 40 μm × 40 μm at the center of each lens, and plotted the surface height variation in Figure 1c,d. A rough surface with 200−400 nm peak-to-valley height variation is seen on the microlens printed without oscillation (Figures 1c and S1a). In contrast, the projection lens oscillation smoothens the microlens surface, and reduces the surface height variation within a range of ∼5 nm (Figures 1d and S1b). Through further mathematical statistics, the surface roughness is quantified by the root mean square value which is 0.91 nm for the microlenses printed with oscillation. This quantitative comparison on the surface roughness confirms that the projection lens oscillation is an effective approach to smoothen the surface of microlens array fabricated by the DLP-based 3D printing system.

Because the projection lens oscillation effectively improves surface smoothness of DLP-fabricated microlens arrays, it is essential to identify the optimal oscillation parameters. Note that in the current oscillation system, the oscillation frequency and amplitude are coupled and have a reciprocal relation. To investigate the effect of oscillation frequency/amplitude, we printed six groups of 3 × 3 microlens (diameter of each lens: 540 μm) arrays with gradually ramped frequency from 0 to 400 Hz. The corresponding oscillation amplitude was characterized by measuring the central offset of the microlens. Figure 1e presents the top view images of these printed samples. It is seen that when the oscillation is off (frequency is 0 Hz), the fabricated microlenses perfectly reproduce the circular shape of the grayscale input. However, when a 100 Hz oscillation is applied, the printed microlenses are distorted into "peanut shape" along the diagonal oscillation direction. This is because at a frequency of 100 Hz, the oscillation amplitude is 220 μm (Figure 1f) which is 22 times of the pixel and 41% of the lens diameter. The excessively large oscillation amplitude severely distorts printed structures. Because the increase in frequency results in a decrease in amplitude (Figure 1f), we find that when the frequency is greater than 200 Hz, the circular distortion disappears (Figure 1e) as the amplitude is 22 μm which is about 2 times of the pixel size. We further conducted AFM measurements to investigate the effect of oscillation frequency/amplitude on the surface roughness of printed microlenses. As shown in Figure 1f, the increase in the oscillation frequency from 0 to 200 Hz leads to a smoother lens surface. However, when the frequency is higher than 200 Hz, the surface roughness starts to worsen. This is because the

DOI: 10.1021/acsami.9b14692
ACS Appl. Mater. Interfaces XXXX, XXX, XXX−XXX

oscillation amplitude is reduced into the size of one pixel or even smaller, which is insufficient to completely smear the pattern formed by discrete pixels and erase the dark grids between pixels. Therefore, after synthetically considering the effect of oscillation on the printing shape fidelity and surface roughness, we decided to use 200 Hz as the oscillation frequency for printing all microlens arrays.

In addition to surface roughness, the lens profile plays another key role in the optical performance of a microlens. Using the oscillation-assisted DLP-based 3D printing system, we can print microlens arrays with different profiles and curvatures by projecting computationally designed grayscale UV patterns with corresponding light intensity and exposure time. To investigate the effect of grayscale distribution, we employed three different grayscale circular patterns (Figure 2a) to fabricate microlens arrays under the same light intensity (4.0 $mW{\cdot}cm^{-2}$) and exposure time (1.5 s). The generation method of the grayscale map is detailed in Supporting Information and Figure S2. Comparing the lens profiles presented in Figure 2a, we find that a uniform exposure yields a relatively flat surface, and the increase in the grayscale gradient leads to a higher curvature of printed lens.

We further investigate the effect of exposure time on the lens profile by projecting the pattern of grayscale 2 which gives a semispherical profile with exposure times of 1.0, 1.5, and 2.0 s under the same light intensity of 4.0 $mW{\cdot}cm^{-2}$. As shown in Figure 2b, the increase in exposure time enlarges the lens profile in both radial and height directions. A similar trend can be found in the case where the light intensity is increased under a fixed exposure time of 2.0 s (Figure S3). However, as long as the total exposure energies (light intensity × exposure time) are the same, different combinations of light intensity and exposure time yield approximately identical profiles (Figure 2c).

In order to better assist the grayscale map design for microlens array fabrication, we develop a theoretical model that utilizes the Gaussian distribution to describe the light intensity distribution from each individual pixel, and the Beer–Lambert law integrated with photopolymerization kinetic equations to model the spatial–temporal variations of light intensity and the concentrations of chemical species such as the photo initiator, monomer and free radical in the polymer solution. Because we model the process of printing spherical lenses, due to the axial symmetry, we can simplify the 3D problem into a two-dimensional one where the x-axis represents the radial direction of a printed lens and the z-axis denotes the height direction. Assuming that n pixels form the diameter of a lens, the light intensity $I(x)$ at an arbitrary spot along the x-axis can be calculated based on the summation of the Gaussian distributed light beams from each pixel: $I(x) = \sum_{i=1}^{n} I_{peak}(x_i)\exp[-(x - x_i)^2 \cdot w_0^{-2}]$, where $I_{peak}(x_i)$ is peak intensity of the i-th pixel and w_0 is Gaussian radius. When UV light penetrates polymer solution, its intensity $I(z,t)$ attenuates by following the one-dimensional Beer–Lambert law:[33] $\partial I(z,t)/\partial z = -\alpha C_I(z,t) I(z,t)$, where α is molar absorptivity, and $C_I(z,t)$ is concentration of the photo initiator which is correlated with the free radical concentration $C_R(z,t)$ and unreacted monomer concentration $C_M(z,t)$ based on the photopolymerization kinetic equations. We solve all the spatial–temporal dependent variables using the finite difference method and calculate the degree of polymerization $p(z,t)$ through $p(z,t) = 1 - C_M(z,t)/C_M(z,0)$ which is used to predict lens profile by plotting the contour where $p(z,t)$ is 0.8.[34] More details regarding the model description are given in Supporting Information and Figure S4. The developed theoretical model is validated by comparing the experimental results with theoretical predictions in Figures 2a,b and S3.

In addition to profile prediction, the developed theoretical model can be inversely used to design grayscale maps for customized microlens profiles. Figure 2d presents the computationally designed grayscale maps for three spherical convex surfaces with same diameter (400 μm) and different heights (120, 80, and 40 μm). It is seen that under the same curing condition, the lens with larger curvature requires a broader grayscale range and smaller exposure area. Moreover, the theoretical model can also be used to design grayscale maps for concave lenses where the light intensity gradually decreases from the edge to the center (Figure 2e). Details of the computational design could be found in Supporting Information and Figure S5.

Using the identified optimal oscillation frequency, predefined curing conditions, and computationally designed grayscale pattern, we printed microlens arrays with a focal length of 650 μm, and tested their optical performance on an optical characterization setup schematically shown in Figure 3a. A microlens array is mounted on a customized sample holder, and a diffusive light beam sequentially passes through a photo-mask and the microlens array which forms a real/virtual image captured by the CCD of a digital microscope depending on the relation between object distance and focal length.

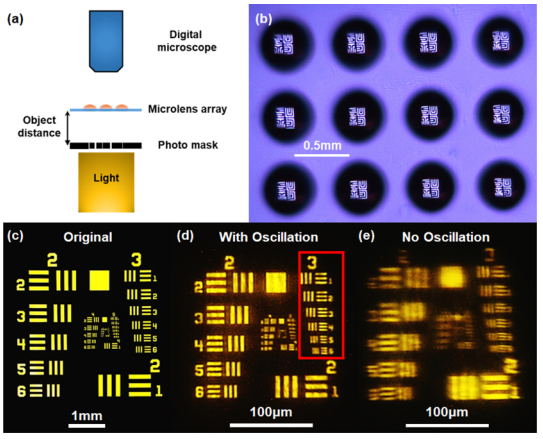

Figure 3. Optical performance of the microlens array fabricated by oscillation-assisted DLP. (a) Schematic of the optical setup. (b) Array of miniaturized SUTD logo images formed by the fabricated microlens array. (c) Original pattern of the USAF1951 resolution test target (group 2–7). (d) Miniaturized image of the USAF1951 target pattern formed by the microlens fabricated under an oscillation frequency of 200 Hz. (e) Miniaturized image of the USAF1951 target pattern formed by the microlens fabricated without oscillation of projection lens.

To assess the uniformity of the focal length in a microlens array, a 3D-printed hollow-carved SUTD logo was placed below the microlens array with an object distance of 40 mm. Because the object distance was far greater than the focal length of the microlenses, upon illumination, an array of miniaturized SUTD logo images formed above the microlens array and was captured by the microscope. It is seen in Figure 3b that the miniaturized logo images are evenly spaced with

DOI: 10.1021/acsami.9b14692
ACS Appl. Mater. Interfaces XXXX, XXX, XXX–XXX

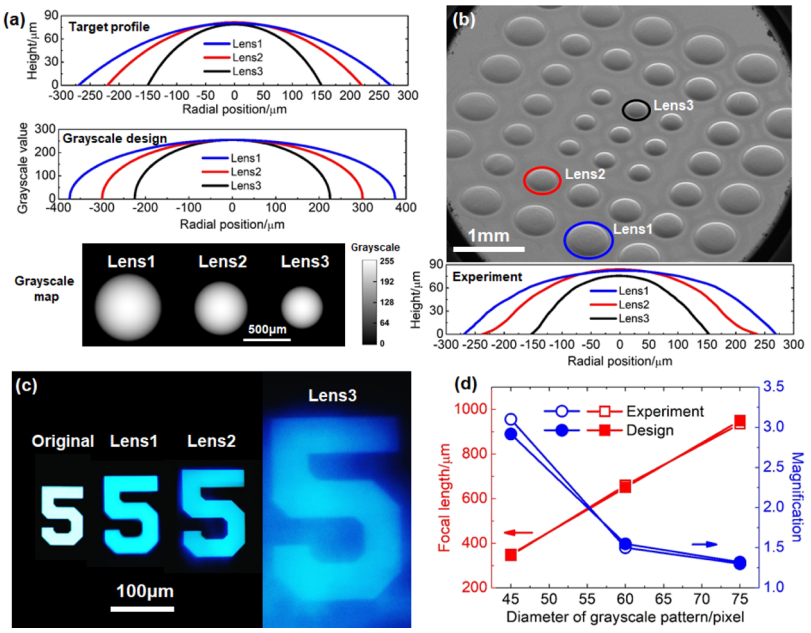

Figure 4. Plano-convex microlens array with varisized microlenses. (a) Design of convex microlenses with the same height and different focal lengths. The target lens profiles, computationally designed grayscale distributions and corresponding grayscale maps are, respectively, presented. (b) SEM image of the microlenses with mixed size and the measured lens profiles. (c) Original pattern of number "5" in USAF1951 resolution test target (group 5) and magnified images of the number "5" pattern formed by the microlenses with different focal lengths. (d) Focal length and magnification of the microlenses with various diameter sizes.

similar size and sharpness, which validates the uniformity of focal length in a printed microlens array.

The imaging resolution of fabricated microlens arrays is further evaluated using the negative USAF1951 resolution test chart (Thorlabs, NJ, USA), which has 6 groups of patterns from +2 to +7. Each group of pattern consists of 6 elements and a highest resolution of 2.19 μm per line is offered in group +7. Figure 3c presents the original test chart pattern captured by a microscope. The test chart patterns are then miniaturized by 21.4 times after placing the printed microlens array 20 mm (object distance) above the test chart. As shown in Figure 3d, the bars in element 6 of group 3 can still be clearly seen after 21.4 times demagnification from 35.08 μm line width to 1.639 μm. In contrast, the image formed by a microlens array fabricated by using the same grayscale pattern but without oscillation is blurry and lacking in resolving power (Figure 3e). This again demonstrates that the projection lens oscillation plays a key role in the optical performance of microlens arrays fabricated on a DLP-based 3D printing system.

The DLP-based 3D printing affords remarkable flexibility to the fabrication of microlens arrays, which enables us to print microlenses with different sizes, geometries, and profiles upon one single UV exposure with different grayscale patterns. To demonstrate this fabrication flexibility, we printed a microlens array consisting of microlenses with the same height (80 μm) but different focal lengths (lens 1: 950 μm, lens 2: 650 μm, lens 3: 350 μm). Figure 4a shows the target lens profiles with diameters of 540 μm (lens 1), 440 μm (lens 2), and 300 μm (lens 3). Determination of the target profiles could be found in Supporting Information. The aforementioned computational design process provides the corresponding grayscale patterns for the target profiles. Figure 4b presents the SEM image of the printed microlens array and the measured microlens profiles which shows good agreement with the corresponding target profiles as shown in Figure 4a. To demonstrate the visual images formed by this microlens array, we placed a negative USAF1951 resolution test target 230 μm below the microlens array (object distance which is smaller than any focal length) and selected the number "5" in group 5 (Figure 4c) as the target pattern. By slowly lowering the distance between the digital microscope and the microlens array, we successively found three virtual images (Figure 4c) formed by lens 1, 2, and 3 with magnifications of 1.3, 1.5, and 3.1, respectively. We further compare the measured magnifications with theoretical ones defined by $M = f/(f - p)$ where f is the focal length and p is the object distance. Good agreement between the measured and predicted magnifications validates the printing fidelity of the proposed fabrication approach (Figure 4d).

Moreover, the high fabrication flexibility even allows us to fabricate convex and concave microlens together upon one single UV exposure. Figure 5a presents the designed grayscale map for fabricating a triangle array of 6 concave microlenses surrounded by fifteen convex ones. Distinguished from the design of a convex microlens, a concave microlens requires a circular pattern with brighter edge and darker interior. Figure 5b shows the SEM image of the printed hybrid concave–convex microlens array whose optical performance was evaluated by observing the 6th and 7th groups of patterns in the USAF1951 resolution test target. As shown in Figure 5c–e, with an object distance of 230 μm, the concave microlens demagnifies the original patterns, while the convex microlens produces a magnified virtual image.

Relative to the other fabrication method such as the thermal reflow of photoresist and direct laser writing, our oscillation-assisted DLP-based printing method is energy- and time-efficient (short UV exposure in the order of seconds) without the degradation of optical performance, which is convenient for commercialization and deployment into mass production. There exist opportunities to add further functionalities such as durability, robustness, and damage resistance to the microlens

DOI: 10.1021/acsami.9b14692
ACS Appl. Mater. Interfaces XXXX, XXX, XXX–XXX

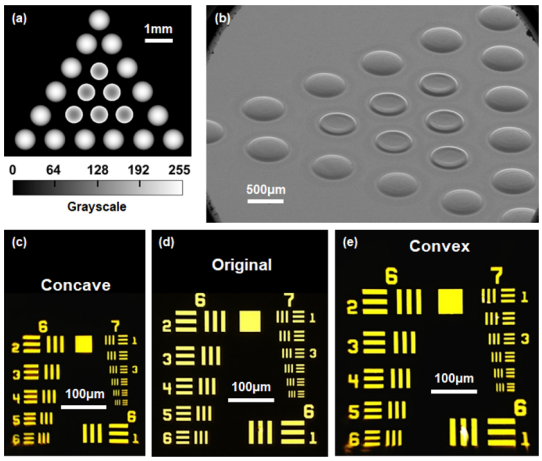

Figure 5. Triangular array of hybrid microlenses. (a) Grayscale map with the hybrid grayscale design. (b) SEM image of the hybrid microlens array. (c) Miniaturized image of the USAF1951 target pattern (group 6−7) formed by the concave microlens. (d) Original pattern of the USAF1951 resolution test target (group 6−7). (e) Magnified image of the USAF1951 target pattern (group 6−7) formed by the convex microlens.

arrays by the oscillation-assisted DLP-based printing method, namely, by infusing silica nanoparticles into the photopolymer matrix followed by postsintering,[35] or adding protective carbon or ceramic coatings.

CONCLUSIONS

In summary, this work reports an oscillation-assisted DLP-based printing system that enables ultrafast (1−3 s) and flexible fabrication of optically smooth microlens arrays. With an optimized oscillation condition and computationally designed grayscale map, microlenses with various sizes and profiles can be simultaneously created with good shape fidelity, low surface roughness (1 nm), and high imaging resolution (1.639 μm linewidth). The rapid fabrication speed and high design flexibility offer significant advantages over existing microlens fabrication techniques and provide instructive inspirations for mass production fields with high demands for ultra-smooth surfaces.

EXPERIMENTAL SECTION

Materials. Monomer 1,6-hexanediol diacrylate (HDDA) and photo initiator diphenyl(2,4,6-trimethylbenzoyl) phosphine oxide (TPO) were purchased from Sigma-Aldrich (St. Louis, MO, USA) and used without further purification. The photocurable solution was prepared by adding TPO into HDDA with a concentration of 5 wt % followed by mixing on the magnetic stirrer (C-MAG HS 7 digital, IKA, Germany) at room temperature for 6 h until full dissolution. The refraction index of the cross-linked HDDA was measured to be 1.52.[36]

Fabrication. A ∼0.1 mL drop of photocurable solution atop a microscope cover glass (24 mm × 24 mm × 0.23 mm) was placed over the fixed glass plate of the platform positioned at the focal plane of the DLP projector (CEL5500, Digital Light Innovations, Austin, TX, USA). Upon starting the vibration generator (Mode U56001, 3B Scientific, Germany), function generator (Mode FG100-1009956, 3B Scientific, Germany), and UV projector, an oscillated grayscale bitmap was projected onto the photocurable resin under a given light intensity and exposure time controlled by a customized LabVIEW (National Instruments, Austin, TX) code. The UV irradiation triggers photopolymerization of the solution and the gradient of the light intensity generated by the grayscale map facilitates the formation of smooth microlens profiles. When the projection was complete, the residual uncured solution was removed by air jetting to prevent the lens surface from being deteriorated by UV postcuring.

Characterization. SEM images of the gold-sputtered microlens samples were taken by the field-emission SEM(JSM-7600F, JEOL Ltd, Tokyo, Japan). AFM scanning was conducted on an atomic force microscope (MFP-3D Origin, Asylum Research, CA, USA). Surface roughness of the microlens samples was obtained by using the flatten command in which a second order polynomial surface was employed to fit the lens profile and subtracted from the original height data. The optical performance of the microlens arrays was characterized by the digital microscope (RH-8800, Hirox Co Ltd., Tokyo, Japan).

ASSOCIATED CONTENT

Supporting Information

The Supporting Information is available free of charge on the ACS Publications website at DOI: 10.1021/acsami.9b14692.

Generation of the grayscale map; modeling; computational design of grayscale map for target profile; and determination of lens geometry (PDF)

AUTHOR INFORMATION

Corresponding Author

*E-mail: geq@sustech.edu.cn.

ORCID

Qi Ge: 0000-0002-8666-8532

Author Contributions

C.Y. and K.K. contributed equally to this work. C.Y., K.K., Z.C., and Q.G. conceived the ideas and designed research. C.Y., K.K., S.P., C.J.N., and P.V.A. contributed to the building of the printing system. C.Y. and D.W. contributed to the development of the theoretical model. C.Y., K.K., and S.P. carried out the experiments. C.Y., S.P., and B.Z. prepared the polymer solution. C.Y. and Q.G. drafted the manuscript. C.Y., K.K., and Q.G. contributed to the writing of the manuscript.

Notes

The authors declare no competing financial interest.

ACKNOWLEDGMENTS

We gratefully acknowledge the grant (RGDM1830206) from SUTD Digital Manufacturing and Design Centre (DManD) funded by the Singapore National Research Foundation. Q.G. acknowledges the research startup grant (Y01336121) by Shenzhen municipal government and the research startup grant (Y01336221) support by Southern University of Science and Technology (SUSTech), and the support by the Centers for Mechanical Engineering Research and Education at MIT and SUSTech.

REFERENCES

(1) Hou, T.; Zheng, C.; Bai, S.; Ma, Q.; Bridges, D.; Hu, A.; Duley, W. W. Fabrication, Characterization, and Applications of Microlenses. *Appl. Opt.* **2015**, *54*, 7366−7376.

(2) Camposeo, A.; Persano, L.; Farsari, M.; Pisignano, D. Additive Manufacturing: Applications and Directions in Photonics and Optoelectronics. *Adv. Opt. Mater.* **2019**, *7*, 1800419.

(3) Hutley, M.; Stevens, R.; Daly, D. Microlens Arrays. *Phys. World* **1991**, *4*, 27−35.

(4) Song, Y. M.; Xie, Y.; Malyarchuk, V.; Xiao, J.; Jung, I.; Choi, K.-J.; Liu, Z.; Park, H.; Lu, C.; Kim, R.-H.; Li, R.; Crozier, K. B.; Huang, Y.; Rogers, J. A. Digital Cameras with Designs Inspired by the Arthropod Eye. *Nature* **2013**, *497*, 95−99.

(5) Motamedi, M. E.; Tennant, W. E.; Sankur, H. O.; Melendes, R.; Gluck, N. S.; Park, S.; Arias, J. M.; Bajaj, J.; Pasko, J. G.; McLevige, W.

DOI: 10.1021/acsami.9b14692
ACS Appl. Mater. Interfaces XXXX, XXX, XXX−XXX

V.; Zandian, M.; Hall, R. L.; Richardson, P. D. Micro-Optic Integration with Focal Plane Arrays. *Opt. Eng.* **1997**, *36*, 1374−1381.
(6) Artzner, G. E. Microlens Arrays for Shack-Hartmann Wave-Front Sensors. *Opt. Eng.* **1992**, *31*, 1311−1322.
(7) Park, E.-H.; Kim, M.-J.; Kwon, Y.-S. Microlens for Efficient Coupling between LED and Optical Fiber. *IEEE Photonics Technol. Lett.* **1999**, *11*, 439−441.
(8) Li, Z.; Wang, X.; Shen, Z.; Lu, J.; Ni, X. Mechanisms for the Millisecond Laser-Induced Functional Damage to Silicon Charge-Coupled Imaging Sensors. *Appl. Opt.* **2015**, *54*, 378−388.
(9) Zhou, X.; Peng, Y.; Peng, R.; Zeng, X.; Zhang, Y.-a.; Guo, T. Fabrication of Large-Scale Microlens Arrays Based on Screen Printing for Integral Imaging 3D Display. *ACS Appl. Mater. Interfaces* **2016**, *8*, 24248−24255.
(10) Wu, M.-H.; Whitesides, G. M. Fabrication of Two-Dimensional Arrays of Microlenses and Their Applications in Photolithography. *J. Micromech. Microeng.* **2002**, *12*, 747−758.
(11) Arai, J.; Kawai, H.; Okano, F. Microlens Arrays for Integral Imaging System. *Appl. Opt.* **2006**, *45*, 9066−9078.
(12) Nussbaum, P.; Völkel, R.; Herzig, H. P.; Eisner, M.; Haselbeck, S. Design, Fabrication and Testing of Microlens Arrays for Sensors and Microsystems. *Pure Appl. Opt.* **1997**, *6*, 617−636.
(13) Daly, D.; Stevens, R. F.; Hutley, M. C.; Davies, N. The Manufacture of Microlenses by Melting Photoresist. *Meas. Sci. Technol.* **1990**, *1*, 759−766.
(14) Jung, H.; Jeong, K.-H. Monolithic Polymer Microlens Arrays with High Numerical Aperture and High Packing Density. *ACS Appl. Mater. Interfaces* **2015**, *7*, 2160−2165.
(15) Kim, J. Y.; Brauer, N. B.; Fakhfouri, V.; Boiko, D. L.; Charbon, E.; Grutzner, G.; Brugger, J. Hybrid Polymer Microlens Arrays with High Numerical Apertures Fabricated Using Simple Ink-Jet Printing Technique. *Opt. Mater. Express* **2011**, *1*, 259−269.
(16) Gissibl, T.; Thiele, S.; Herkommer, A.; Giessen, H. Two-Photon Direct Laser Writing of Ultracompact Multi-Lens Objectives. *Nat. Photonics* **2016**, *10*, 554−560.
(17) Wu, D.; Wu, S.-Z.; Niu, L.-G.; Chen, Q.-D.; Wang, R.; Song, J.-F.; Fang, H.-H.; Sun, H.-B. High Numerical Aperture Microlens Arrays of Close Packing. *Appl. Phys. Lett.* **2010**, *97*, 031109.
(18) Florian, C.; Piazza, S.; Diaspro, A.; Serra, P.; Duocastella, M. Direct Laser Printing of Tailored Polymeric Microlenses. *ACS Appl. Mater. Interfaces* **2016**, *8*, 17028−17032.
(19) Yong, J.; Chen, F.; Yang, Q.; Du, G.; Bian, H.; Zhang, D.; Si, J.; Yun, F.; Hou, X. Rapid Fabrication of Large-Area Concave Microlens Arrays on PDMS by a Femtosecond Laser. *ACS Appl. Mater. Interfaces* **2013**, *5*, 9382−9385.
(20) Pantelis, P.; McCartney, D. J. Polymer Microlens Arrays. *Pure Appl. Opt.* **1994**, *3*, 103−108.
(21) Chan, E. P.; Crosby, A. J. Fabricating Microlens Arrays by Surface Wrinkling. *Adv. Mater.* **2006**, *18*, 3238−3242.
(22) Dong, L.; Agarwal, A. K.; Beebe, D. J.; Jiang, H. Adaptive Liquid Microlenses Activated by Stimuli-Responsive Hydrogels. *Nature* **2006**, *442*, 551−554.
(23) Jiang, C.; Li, X.; Tian, H.; Wang, C.; Shao, J.; Ding, Y.; Wang, L. Lateral Flow through a Parallel Gap Driven by Surface Hydrophilicity and Liquid Edge Pinning for Creating Microlens Array. *ACS Appl. Mater. Interfaces* **2014**, *6*, 18450−18456.
(24) Sun, C.; Fang, N.; Wu, D. M.; Zhang, X. Projection Micro-Stereolithography Using Digital Micro-Mirror Dynamic Mask. *Sens. Actuators, A* **2005**, *121*, 113−120.
(25) Ge, Q.; Sakhaei, A. H.; Lee, H.; Dunn, C. K.; Fang, N. X.; Dunn, M. L. Multimaterial 4D Printing with Tailorable Shape Memory Polymers. *Sci. Rep.* **2016**, *6*, 31110.
(26) Tumbleston, J. R.; Shirvanyants, D.; Ermoshkin, N.; Janusziewicz, R.; Johnson, A. R.; Kelly, D.; Chen, K.; Pinschmidt, R.; Rolland, J. P.; Ermoshkin, A.; Samulski, E. T.; DeSimone, J. M. Continuous Liquid Interface Production of 3D Objects. *Science* **2015**, *347*, 1349−1352.
(27) Zheng, X.; Lee, H.; Weisgraber, T. H.; Shusteff, M.; DeOtte, J.; Duoss, E. B.; Kuntz, J. D.; Biener, M. M.; Ge, Q.; Jackson, J. A.; Kucheyev, S. O.; Fang, N. X.; Spadaccini, C. M. Ultralight, Ultrastiff Mechanical Metamaterials. *Science* **2014**, *344*, 1373−1377.
(28) Patel, D. K.; Sakhaei, A. H.; Layani, M.; Zhang, B.; Ge, Q.; Magdassi, S. Highly Stretchable and UV Curable Elastomers for Digital Light Processing Based 3D Printing. *Adv. Mater.* **2017**, *29*, 1606000.
(29) Kowsari, K.; Akbari, S.; Wang, D.; Fang, N. X.; Ge, Q. High-Efficiency High-Resolution Multimaterial Fabrication for Digital Light Processing-Based Three-Dimensional Printing. *3D Print. Addit. Manuf.* **2018**, *5*, 185−193.
(30) Lu, Y.; Chen, S. Direct Write of Microlens Array Using Digital Projection Photopolymerization. *Appl. Phys. Lett.* **2008**, *92*, 041109.
(31) Chen, X.; Liu, W.; Dong, B.; Lee, J.; Ware, H. O. T.; Zhang, H. F.; Sun, C. High-Speed 3D Printing of Millimeter-Size Customized Aspheric Imaging Lenses with Sub 7 nm Surface Roughness. *Adv. Mater.* **2018**, *30*, 1705683.
(32) Gao, Y.; He, S.; Luo, N.; Rao, Y. Research on Dynamical-Gradual Greyscale Digital Mask Lithography. *J. Mod. Opt.* **2011**, *58*, 573−579.
(33) Wu, J.; Zhao, Z.; Hamel, C. M.; Mu, X.; Kuang, X.; Guo, Z.; Qi, H. J. Evolution of Material Properties during Free Radical Photopolymerization. *J. Mech. Phys. Solids* **2018**, *112*, 25−49.
(34) Torres-Knoop, A.; Kryven, I.; Schamboeck, V.; Iedema, P. D. Modeling the Free-Radical Polymerization of Hexanediol Diacrylate (HDDA): a Molecular Dynamics and Graph Theory Approach. *Soft Matter* **2018**, *14*, 3404−3414.
(35) Kotz, F.; Arnold, K.; Bauer, W.; Schild, D.; Keller, N.; Sachsenheimer, K.; Nargang, T. M.; Richter, C.; Helmer, D.; Rapp, B. E. Three-Dimensional Printing of Transparent Fused Silica Glass. *Nature* **2017**, *544*, 337−339.
(36) Kowsari, K.; Zhang, B.; Panjwani, S.; Chen, Z.; Hingorani, H.; Akbari, S.; Fang, N. X.; Ge, Q. Photopolymer Formulation to Minimize Feature Size, Surface Roughness, and Stair-Stepping in Digital Light Processing-Based Three-Dimensional Printing. *Addit. Manuf.* **2018**, *24*, 627−638.

DOI: 10.1021/acsami.9b14692
ACS Appl. Mater. Interfaces XXXX, XXX, XXX−XXX